Since January 2020 Elsevier has created a COVID-19 resource centre with free information in English and Mandarin on the novel coronavirus COVID-19. The COVID-19 resource centre is hosted on Elsevier Connect, the company's public news and information website.

Journal Pre-proof

Response of $PM_{2.5}$-bound elemental species to emission variations and associated health risk assessment during the COVID-19 pandemic in a coastal megacity

Guochen Wang , Kan Huang , Qingyan Fu , Jia Chen , Juntao Huo , Qianbiao Zhao , Yusen Duan , Yanfen Lin , Fan Yang , Wenjie Zhang , Hao Li , Jian Xu , Xiaofei Qin , Na Zhao , Congrui Deng

PII: S1001-0742(21)00421-6
DOI: https://doi.org/10.1016/j.jes.2021.10.005
Reference: JES 2756

To appear in: *Journal of Environmental Sciences*

Received date: 12 March 2021
Revised date: 19 September 2021
Accepted date: 6 October 2021

Please cite this article as: Guochen Wang , Kan Huang , Qingyan Fu , Jia Chen , Juntao Huo , Qianbiao Zhao , Yusen Duan , Yanfen Lin , Fan Yang , Wenjie Zhang , Hao Li , Jian Xu , Xiaofei Qin , Na Zhao , Congrui Deng , Response of $PM_{2.5}$-bound elemental species to emission variations and associated health risk assessment during the COVID-19 pandemic in a coastal megacity, *Journal of Environmental Sciences* (2021), doi: https://doi.org/10.1016/j.jes.2021.10.005

Response of $PM_{2.5}$-bound elemental species to emission variations and associated health risk assessment during the COVID-19 pandemic in a coastal megacity

Guochen Wang[1], Kan Huang[1,5,6,*] huangkan@fudan.edu.cn, Qingyan Fu[2,*] qingyanf@sheemc.cn, Jia Chen[1], Juntao Huo[2], Qianbiao Zhao[2], Yusen Duan[2], Yanfen Lin[2], Fan Yang[3], Wenjie Zhang[4], Hao Li[1], Jian Xu[1], Xiaofei Qin[1], Na Zhao[1], Congrui Deng[1]

[1]Shanghai Key Laboratory of Atmospheric Particle Pollution and Prevention (LAP[3]), Department of Environmental Science and Engineering, Fudan University, Shanghai 200433, China. E-mail: 18110740052@fudan.edu.cn

[2]Shanghai Environmental Monitoring Center, Shanghai, 200030, China

[3]Pudong New District Environmental Monitoring Station, Shanghai, 200122, China

[4]Chinese Research Academy of Environmental Sciences, Beijing, 100012, China

[5]International Center of Excellence on Risk Interconnectivity and Governance on Weather/Climate Extremes Impact and Public Health, Fudan University, Shanghai 200433, China

[6]Institute of Eco-Chongming (IEC), Shanghai, 202162, China

[*]Corresponding author: K. Huang, Q.Y. Fu

Abstract

The coronavirus (COVID-19) pandemic is disrupting the world from many aspects. In this study, the impact of emission variations on $PM_{2.5}$-bound elemental species and health risks associated to inhalation exposure has been analyzed based on real-time measurements at a remote coastal site in Shanghai during the pandemic. Most trace elemental species decreased significantly and displayed almost no diel peaks during the lockdown. After the lockdown, they rebounded rapidly, of which V and Ni even exceeded the levels before the lockdown, suggesting the recovery of both inland and shipping activities. Five sources were identified based on receptor modeling. Coal combustion accounted for more than 70% of the measured elemental concentrations before and during the lockdown. Shipping emissions, mineral/fugitive dust, and waste incineration all showed elevated contributions after the lockdown. The total non-carcinogenic risk (HQ) for the target elements exceeded the risk threshold for both children and adults with chloride as the predominant species contributing to HQ. Whereas, the total carcinogenic risk (TR) for adults was above the acceptable level and

much higher than that for children. Waste incineration was the largest contributor to HQ, while manufacture processing and coal combustion were the main sources of TR. Lockdown control measures were beneficial for lowering the carcinogenic risk while unexpectedly increased the non-carcinogenic risk. From the perspective of health effects, priorities of control measures should be given to waste incineration, manufacture processing, and coal combustion. A balanced way should be reached between both lowering the levels of air pollutants and their health risks.

Graphical Abstract Graphical Abstract

.

Keywords

COVID-19 lockdown; $PM_{2.5}$-bound elemental species; Source apportionment; Health risk; Shanghai

Introduction

China witnessed an unknown pathogen outbreak in the end of December, 2019 (Zhu et al., 2020; Li et al., 2020; Zhou et al., 2020). A novel coronavirus, namely COVID-2019, was confirmed by World Health Organization (WHO) and proved to be the cause of this public health crisis and strongly hit the growth of the world economy (WHO, 2020). As the etiological agent (Wu et al., 2020), human-to-human transmission of the novel coronavirus has been confirmed (https://apnews.com/14d7dcffa205d9022fa9ea593bb2a8c5, latest accessed on 7 June, 2020). To date, 225,213,795 confirmed cases in the world and 107,480 confirmed cases in China were recorded according to the live updates released by Johns Hopkins University (https://coronavirus.jhu.edu/map.html, latest accessed on 14, September 2021).

To control and prevent further spread of the deadly virus, the Chinese government have taken very stringent control measures to cut off the dispersion of COVID-19 virus. On 23, January 2020, China also raised its national public health response to the highest state of emergency, i.e. the level I response. Due to the nationwide reduction of human activities during the COVID-19 lockdown, the economy in China has shrunk dramatically and accompanied by a strong reduction of pollutant emissions. As a result, air quality has been witnessed substantial changes, especially from the primary air pollutants in China (Shi et al., 2020; Wang et al., 2020). For example, the TROPOMI instrument boarded on the Sentinel 5P satellite observed the decrease of tropospheric NO_2 columns over Chinese cities by about 40% in January–April

2020, compared to the same period in 2019 (Bauwens et al., 2020). Huang et al. (2020) also showed that the overall reduction of simulated NO_x was about 60−70% in eastern China, of which 70−80% can be attributed to traffic emissions and 20−25% to industries and power plants. Li et al. (2020) suggested that concentrations of air pollutants like SO_2, NO_x, $PM_{2.5}$, and VOCs were reduced by 26%, 47%, 46%, and 57%, respectively, during the most stringent COVID-19 lockdown period over the Yangtze River Delta region (YRD).

As a result of the global pandemic of COVID-19, public health-related topics have rocketed to a new height. Among these concerns, air pollution has become a hot issue which was focused by health experts and the public. According to the report from *State of Global Air 2020*, air pollution has emerged to the 4th leading risk factor for early death worldwide in 2019 (Health Effects Institute, 2020). Although trace elemental species compose a small proportion in $PM_{2.5}$, they have great harm to human health for many metallic metals have noncarcinogenic and carcinogenic risks, such as As (arsenic), Cr (chromium), Ni (nickel), Mn (manganese) and so on (Slezakova et al., 2014). For example, the International Agency for Research on Cancer (IARC) has designated As, Cd, hexavalent chromium, lead-related compounds, and nickel-related compounds as carcinogens to public health (IARC, 2006, 2012). As the impact of heavy metals on human health risk is chronic and long-term, more special attention should be paid to those $PM_{2.5}$-bound substances.

Till now, most efforts have been devoted to evaluating the response of air quality changes to the stringent control measures over urban areas and much attentions have been paid to the mechanisms of secondary aerosol formation during pandemic and quarantine periods (Huang et al., 2020; Li et al., 2020). However, little is known about how would the trace elemental species in $PM_{2.5}$ respond to the varying emissions and the influence of emission changes on human health risk during the COVID-19 pandemic. In this study, real-time measurements of atmospheric trace elemental species in $PM_{2.5}$ at a remote coastal site in Shanghai were conducted to pinpoint the variations of different emission sources. Also, the influences of air pollution on human health before, during, and after the lockdown were assessed. What's more, this study also provided insights for air pollution controls from the perspective of both pollution sources and human health.

1 Methodology

1.1 Observational site

One remote site, namely, Dongtan site is setup at the Chongming Island, an agricultural district of Shanghai (**Fig. 1**). This site is located in the Dongtan Wetland Park at the very

eastern tip of Chongming Island. It is surrounded by wetland and different types of vegetations with almost no human activities around. Due to its unique geographic location at the junction of the Yangtze River and the East China Sea, it is an ideal site for evaluating the impacts from inland and marine shipping activities. In addition, an urban site, Pudong, was used to compare with Dongtan.

1.2 Instrumentation

Hourly ambient mass concentrations of 19 trace elements (Si, S, Cl, K, Ca, V, Cr, Mn, Fe, Ni, Cu, Zn, As, Cd, Ba, Pb, Co, Ti, and Al) and 15 elemental species (Si, K, Ca, V, Cr, Mn, Fe, Ni, Cu, Zn, As, Cd, Ba, Pb, Co) in $PM_{2.5}$ at Dongtan and Pudong, respectively, were measured by a Xact multi-metals monitor (Model Xact™ 625, Cooper Environmental Services LLT, OR, USA). The air samples passed through a $PM_{2.5}$ cyclone inlet at a flow rate of 16.7 L/min and were deposited on a reel-to-reel Teflon filter tape, and then the samples entered into the analysis area for nondestructive energy-dispersive X-ray fluorescence analysis. The minimum detection limits (ng/m^3) for the hourly resolution were: Si (17.80), S (3.16), Cl (1.73), K (1.17), Ca (0.30), V (0.12), Cr (0.12), Mn (0.14), Fe (0.17), Ni (0.10), Cu (0.079), Zn (0.067), As (0.063), Cd (2.5), Ba (0.39), Pb (0.13), Co (0.14) , Ti (0.16), and Al (100). More details about the instrument can be found in Chang et al. (2018).

Meteorological parameters at Dongtan were measured by an automatic meteorological observation instrument (WXT 536, Vaisala, Finland), including temperature (T), relative humidity (RH), wind speed (WS), wind direction (WD), pressure, and precipitation.

1.3 Calculation of enrichment factors (EF)

Enrichment factors (EF) is a simple normalization method, which is widely used to study the enrichment of trace elemental species in aerosol (Gelado-Caballero et al., 2012; Shelley et al., 2015; Zhao et al., 2013). It can eliminate the influence of various variable factors such as meteorological factors and distance from pollution sources. Generally, aluminum (Al) was selected as the reference element for its few anthropogenic pollution sources and good chemical stability in the crust. In this study, the average chemical composition of the upper continental crust (UCC) used was referred from Wedepohl et al. (1995). Therefore, *EF* can be expressed as follows:

$$EF_{[X]} = ([X]/[Al])_{aerosol} / ([X]/[Al])_{crust} \qquad (1)$$

Where $([X]/[Al])_{aerosol}$ and $([X]/[Al])_{crust}$ are the mass concentration ratios of the interest

trace elemental species *[X]* versus the reference element *[Al]* in aerosol and crust, respectively.

1.4 Source apportionment

The source contributions of $PM_{2.5}$-bound trace elemental species were quantitatively analyzed by using an EPA Positive Matrix Factorization (US EPA, 2014) receptor model. PMF is a receptor-based quantitative source apportionment model, which was originally introduced by Paatero and Tapper (1994). The model has been widely used to identify the possible sources of various particulate components. The goal of receptor model is to solve the chemical mass balance between measured species concentrations and source profiles using the least square method (Paatero and Tapper, 1994; Paatero et al., 2014). The measured mass concentration xij can be expressed as:

$$x_{ij} = \sum_{k=1}^{p} g_{ik} f_{kj} + e_{ij} \quad (2)$$

Where, x_{ij} is the mass concentration; g represents measured species concentrations and f denotes source profiles; i is the number of samples; j is the chemical species; p is the total number of pollution sources; k represents a specific pollution source; e_{ij} is the residual for each sample/species.

The uncertainty of data was calculated based on the method detection limit (*MDL*) and determination error fraction (Paatero et al., 2014), which can be calculated as below.

If the concentration of target element is lower than the *MDL*, then,

$$Unc = 5/6\ MDL \quad (3)$$

And if the concentration of target element is higher than the *MDL*, then,

$$Unc = \sqrt{(\text{error fraction} \times C_i)^2 + (0.5 \times MDL)^2} \quad (4)$$

Where, C_i denote the mass concentrations of target elemental species *i*; *Unc* is the data uncertainty. The initial value of the error fraction was set to 10%, which was recommended by previous studies (Liu et al., 2018; Gao et al., 2014; Yang et al., 2016). In addition, 5% of the extra modeling uncertainty was applied to all species.

1.5 Health risk assessment

We assessed individual health risks from elemental species in $PM_{2.5}$ via inhalation. Noncarcinogenic and carcinogenic risks were assessed according to the methodology provided by United States Environmental Protection Agency (USEPA, 2009). Exposure levels of noncarcinogenic risks of each individual species were assessed using the ratio of the

exposure concentration of a single substance over a specified period of time to the reference dose (RfD) of the substance over a similar exposure period. If the exposure level exceeded the threshold of 1.0, potential non-carcinogenic effects may occur (USEPA, 1989). The exposure level was expressed as the non-carcinogenic hazard quotient (*HQ*) and can be derived as below.

$$HQ = \frac{C \times EFr \times ED \times ET \times IR}{RfD \times BW \times AT} \quad (5)$$

Where, *HQ* is non-carcinogenic hazard quotient (unitless); *C* is the concentration of elemental species in $PM_{2.5}$ (mg/m^3); EF_r is the exposure frequency; *ED* is the exposure duration (years), which was set as 3 years for children (3-10) and 20 years for adults (20-59); *ET* is the exposure time (24 hr per day was used in this study); *IR* is the average inhalation rate (m^3/day); *BW* is the average body weight (kg); *AT* is the number of days over which the exposure is averaged (noncarcinogenic risk: 365 days/year × *ED*; carcinogenic risk: 365 days/year × 70 years); *RfD* is the inhalation reference dose (mg/kg/day).

The target carcinogenic risk is assessed as the increased probability of an individual developing cancer through direct inhalation of carcinogens over a lifetime, as a result of exposure to that potential toxic carcinogen. Acceptable risk levels for carcinogens is set at 10^{-6} (USEPA, 1989, 2009), below which no carcinogenic risk can be considered. The target carcinogenic risk is calculated as below.

$$TR = \frac{C \times EFr \times ED \times ET \times IUR}{AT} \quad (6)$$

where, *TR* is the target carcinogenic risk (unitless); *IUR* is the chronic inhalation unit risk ($\mu g/m^3$).

The cumulative noncarcinogenic and carcinogenic risks were also calculated as the sum of the *HQ* and *TR* of all targeted elemental species, respectively. More details about the parameters used in the health risk assessment were summarized in the supplementary material (**Table S1 and S2**). In the atmosphere, Cr has several valence states, such as Cr (Ⅲ) and Cr (VI). Among them, Cr (VI) is regarded as more toxic than the others (US EPA, 2018; Hsu et al., 2016; Chen et al., 2021). Thus, the health risk of Cr should be calculated as the concentration of Cr (VI) rather than as the total Cr concentration. In the study, we assumed a 1:6 ratio of Cr (VI) to Cr (III) based on the USEPA Regional Screening Levels (RSL) (USEPA, 2018). Therefore, Cr divided by 7 is expressed as Cr (VI) when calculating the health risk.

2 Results and discussion

2.1 General description

Three periods were defined based on the starting and ending time of lockdowns, i.e. Pre-Lock (1, January 2020 to 23, January 2020), COVID-Lock (24, January 2020 to 17 February, 2020), and Post-Lock (18, February 2020 to 31 March, 2020). The air quality in Chinese mainland experienced significant changes during the pandemic lockdown periods. For example, the average NO_2 tropospheric column densities displayed strong decreases during the COVID-Lock period in the North China Plain, Yangtze River Delta, Pearl River Delta, and Central China (e.g. Wuhan) as well as over the East China Sea (**Fig. S1**). It is well known that the major sources of NO_x derived from combustion sources, thus the significant reduction of NO_2 columns reflected strongly restrained human activities such as reduced traffic and industrial activities. After the lockdown, the NO_2 columns increased obviously although it still hadn't reached to the level before the lockdown, suggesting a progressive recovery of the economic activities.

2.2 Impact of COVID-19 lockdown on air pollution

2.2.1 Variations of trace elemental species

Fig. 2 shows the variations of mass concentrations of 19 typical trace elements in $PM_{2.5}$ at Dongtan before, during, and after lockdowns. Most trace elements showed decreases during COVID-Lock. As tracers for industries (mainly from manufacture processing), Cr, Mn, Fe, and Zn during COVID-Lock decreased by 60%, 57%, 37%, and 57% compared to Pre-Lock, respectively, suggesting the significant impact of lockdown on lowering the capacity of manufacture processing. Fugitive/mineral dust exhibited a similar pattern, but the variation was not so obvious, of which Ca and Al decreased by 15% and 7%, respectively. As, S, and Pb also showed slight decreases of 10%, 10%, and 28%, respectively. V and Ni are usually considered as typical tracers of shipping emissions (Chang et al., 2018; Zhao et al., 2013; Pandolfi et al., 2011). Shanghai is adjacent to many huge capacity ports, such as Yangshan port, Ningbo-Zhoushan port, and Wusongkou port (**Fig. 1**) and acts as the hub of shipping communication. Hence, the measured V and Ni can mostly reflect the variation of shipping activities. Compared to Pre-Lock, V and Ni decreased by 30% and 27% during COVID-Lock, respectively, suggesting shipping activities were also restrained. According to Shanghai Municipal Bureau of Statistics, the cargo capacity of Shanghai port in January and February, 2020 were 54.95 and 37.19 million tons, which decreased by 14.0% and 18.8% compared to the same month last year (http://tjj.sh.gov.cn/sjxx/index.html). It is worth noting that the

concentration of Cl showed an increase during the lockdown period, indicating that waste incineration increased during the epidemic period. This may be due to the fact that during the epidemic period, the implementation of home quarantine measures led to an increase in family dinners, resulting in a large amount of domestic waste. Those wastes were mainly disposed by combustion, and heavily contributed to the increase of Cl during the epidemic lockdown.

After the lockdown, along with the gradual resumption of work and production, some industries had recovered to the level before the lockdown, resulting in the rebound of anthropogenic emissions. As shown in **Fig. 2**, trace elemental species from industrial processing (Cr, Mn, Fe, and Zn) and shipping emissions (V and Ni) showed rebounds after the lockdown. Among them, V and Ni showed very significant increases of 123% and 48%, even exceeding the concentrations before the lockdown. The statistical data documented that the cargo capacity of Shanghai port in March, 2020 was 54.96 million tons, which increased by 47.8% compared to February, 2020 (http://tjj.sh.gov.cn/sjxx/index.html), revealing that the rebound of V and Ni were mainly ascribed to intensified shipping activities after the lockdown.

Similar variations were also observed at an urban site, Pudong (**Fig. S2**). Cr, Mn, Fe and Zn during COVID-Lock decreased by 76%, 76%, 54% and 63%, respectively, compared to Pre-Lock, and then rebounded and approached to levels before the lockdown. Ca and Si showed the same trend, presenting a strong increase after the lockdown compared to the lockdown period. Unlike Dongtan, V presented a continuously decreasing trend during (19%) and after (12%) the lockdowns, while Ni showed a decreasing (36%) and then increasing (20%) trend, which was due to Pudong is located in urban area and less influenced by shipping emissions.

To evaluate the relative contribution of possible origins (natural or anthropogenic), the enrichment factor (EF) was introduced to pinpoint the enrichment extents of various trace elemental species. As suggested in previous studies, trace elemental species with EF values greater than 10 were regarded as having considerable anthropogenic sources, while those of EF values less than 10 mainly originated from natural sources. **Fig. S3** shows the EFs of major trace elemental species during the three periods. Trace elemental species including Ni, Cu, Cl, Zn, Pb, As, S, and Cd showed EFs > 10, suggesting those trace elemental species were enriched by anthropogenic sources such as shipping emissions, manufacture processing, and coal combustion (Zhao et al., 2013; Gelado-Caballero et al., 2012). Among the three periods, EFs of most trace elemental species exhibited a V-shaped pattern curve, especially those from shipping emissions and manufacturing processing. Compared to Pre-Lock, EFs of most trace

elemental species during the lockdown showed decreases. After the lockdown, EFs increased with different extents. EFs of V and Ni after the lockdown exceeded those during Pre-Lock, indicating the recovery of shipping activities.

2.2.2. Impact of lockdown on diel patterns of trace elemental species

Fig. 3 shows the diel patterns of selected trace elemental species in $PM_{2.5}$ before, during, and after lockdowns.

During Pre-Lock, all trace elemental species showed obvious diel cycles with higher values in the daytime and lower values at night, which can be attributed to the intensive anthropogenic activities in the daytime. As Dongtan was far away from the populous and industrialized areas (**Fig. 1**), the noon peaks of most elements may be due to the transport from various emission sources. The polar plot maps (**Fig. S4**) show that Cr, Mn, Zn, As, Ca, and Fe with higher concentrations were mainly from the southwest during all three periods, corresponding to the directions where Shanghai's heavy industries intensively distributed such as coal-fired power plants, iron steel smelters, petrochemical complex, and nonferrous metal smelters (**Fig. 1**). **Fig. S5** shows that the noon peaks of $PM_{2.5}$ at Dongtan lagged about 2−4 hours relative to that observed at Shanghai urban areas, corroborating the transport characteristics of air pollutants at Dongtan. As a comparison, the peaks of V and Ni occurred in the early morning and late afternoon. Since Dongtan is a remote costal site surrounded by the inland and international shipping channels, the diel patterns of V and Ni should be mainly controlled by the meteorological conditions such as the boundary layer which was shallow in the morning and night while developed more around noon. The diel pattern of wind speed at Dongtan also suggested that the mean wind speed in the daytime was much higher than that at night, suggesting the atmospheric diffusion condition in the daytime was better than that at night (**Fig. 3**). Such a diurnal pattern was similar to that observed at Pudong where all elemental species displayed a decreasing trend during the lockdown, except for V which remained almost constant compared to Pre-Lock (**Fig. S6**).

Compared to Pre-Lock, all species except Cl showed decreases during the lockdown. Specifically, the diel patterns of all the trace elemental species became either flat or irregular without showing discernable peaks. The remarkably reduced anthropogenic emissions from both land and waters during the lockdown were evidently responsible for this. Cl was an exception that showed stronger diel pattern and higher concentrations during the lockdown, which may be related to the increase of waste incineration caused by more domestic waste from living at home during quarantine.

After the lockdown, most trace elemental species except for those from combustion-related sectors rebounded rapidly. Cr, Mn, and Zn resumed their diel patterns although the extents of their diel patterns were much weaker than Pre-Lock, suggesting the recovery of industrial productions was still limited. As for the diel patterns of Ca and Fe, they were as similar as those before the lockdown, indicating that the contribution of fugitive dust increased with the recovery of road traffic after the lockdown. The diel patterns of Vi and Ni returned as similar as those during Pre-Lock and their diel concentrations approached or exceeded those before the lockdown, further corroborating that shipping activities gradually recovered after the lockdown as discussed in Section 2.2.1. In contrast, the diel patterns of S, As, and Pb remained almost invariable without showing discernable peaks, indicating the usage of coal was at a low level.

2.3 Source apportionment of trace elemental species

The PMF receptor model was applied to apportion the sources of measured elemental species. Totally, five sources were identified based on the typical tracers of specific sources (**Fig. 4a**).

The first factor was identified as fugitive/mineral dust. This factor was characterized of high contributions from Si (100.0%), Ca (54.6%), and Ti (57.3%). These elemental species are common chemical compositions of the upper continental crust (UCC) and considered as the tracers of fugitive dust and desert dust (Pandolfi et al., 2011; Visser et al., 2015; Amato et al., 2013; Pérez et al., 2016; Chang et al., 2018;). As far away from the Asian dust source regions, Shanghai is rarely affected by dust. Thus, this factor can be related to road dust/fugitive dust, construction works, and soil erosion.

The second factor was identified as coal combustion with high contributions from S (76.1%), K (67.1%), Pb (71.6%), and As (48.7%). These elements were mainly derived by coal combustion (Okuda et al. 2008; Chang et al., 2018; Tian et al., 2015). In the past, Pb was considered as an indicator of vehicle emissions because of the use of leaded gasoline (Nriagu, 1989). However, with the widespread use of unleaded gasoline in recent years, the content of Pb in fuel oil was low (Čimová et al., 2016; Bartoňová et al., 2019), so Pb was considered to be mainly from coal combustion (Zhang et al., 2013; Wei et al., 2021). K was regarded as the tracer of biomass burning (Cheng et al., 2013; Pachon et al., 2013). However, several studies pointed out that K was also emitted from coal combustion. For example, Yu et al. (2018) showed that K shared good correlations with heavy metals ascribed to coal combustion (e.g., Pb, As, Se, and Zn) and coal combustion was the predominant source of K (45–69%) in

Beijing. Chang et al., (2018) also found that over 50% of K in urban Shanghai was related to coal combustion.

The third factor was identified as shipping emission due to the high contributions from V (94.4%) and Ni (75.9%). V and Ni are mainly produced by fuel oil combustion especially the heavy oil used by ship and crude oil refined by petrochemical industries (Pandolfi et al., 2011; Park et al., 2014; Liu et al., 2018). Located in East Asia, Shanghai is the hub of many international marine routes with the world's largest port-Shanghai port. According to the data released by Shanghai Port Group, the containers in Shanghai port reached 43.5 million TEUs in 2020, ranking first in the world (http://service.shanghai.gov.cn/SHVideo/newvideoshow.aspx?id=40200EF3F2C94872). Thus, V and Ni were mainly from shipping emissions (Zhao et al., 2013; Pérez et al., 2016). In addition, large and medium-sized petrochemical industries were distributed in the east and southwest of Shanghai (**Fig. 1**). Therefore, Dongtan may be also affected by petrochemical industry emissions.

The fourth factor was characterized of high levels of Cr (91.5%), Mn (75.9%), Fe (39.7%), Cu (73.8%), and Zn (56.2%). Cr, Mn, and Fe can be derived from ferrous metal smelting (Amato et al., 2009; Pérez et al., 2016). Cu and Zn are typically considered from metal smelting (Tian et al., 2015). These elemental species are typically released by manufacture processing of both nonferrous metal smelting and ferrous metal smelting (Pandolfi et al., 2011; Chang et al., 2018).

As for the fifth factor, Cl (81%) was the exclusively dominant element. Though Cl could be emitted from coal combustion, typical coal combustion tracers such as S, As, and Pb showed negligible contributions in this factor. Previous studies have shown that waste incineration was an important source of Cl-related emissions (McCulloc et al., 1999; Fu et al., 2018). Liu et al. (2018) estimated that the chlorine related (HCl) emissions from waste incineration in China was around 2.9 Gg in 2012, and the Yangtze River Delta was one of the hot spot regions of chlorine related emissions. Hence, we attributed this factor to waste incineration.

Fig. 4b compares the relative proportions of the identified sources before, during, and after the lockdowns. Although the mass concentrations of most elements during COVID-Lock decreased compared to Pre-Lock, the relative contributions from five sources between these two periods were similar. Coal combustion was the predominant source, accounting for about three-quarters of the measured elements. Manufacture processing and shipping emissions contributed less while waste incineration contributed more during COVID-Lock, reaching about 13%.

After the lockdown, the contributions from shipping emissions and fugitive/mineral dust increased the most. Shipping emissions increased from around 10% to 26%, ranking as the second largest source of trace elements, highlighting the fast growing demand of domestic and international shipping after the lockdown. The enhanced fugitive/mineral dust was partly attributed to the recovery of road traffic after the lockdown. In addition, dust episode originated from north China and transported during Post-Lock (**Fig. S7**), increasing the abundances of crustal elements. The contributions from waste incineration and manufacture processing increased slightly. As a result, the contribution from coal combustion was largely reduced to around 38%.

2.4 Exposure assessment

2.4.1 Elemental species-based health risk assessment

Fig. 5a shows the estimation of non-carcinogenic risk via inhalation exposure from specific elements that had health effects. The total HQ (hazard quotient) for all trace elemental species exceeded the threshold (1.0) during the whole study periods for both children and adults, suggesting a potential health risk. During Pre-Lock, the HQ of the selected elements followed the order of Cl > As > Mn > Al > Ni > Cd > V > Si > Co > Ba > Cr (VI) > Pb > Cu > Zn. It was Cl > As > Mn >Al > Ba > Ni > Cd > Si > V > Co > Pb > Cr (VI) > Cu > Zn during COVID-Lock and Cl > As > Mn > Si > Ni > Al > Cd > V > Co > Cr (VI) > Ba > Pb > Cu > Zn during Post-Lock, respectively. Obviously, Cl had the greatest contribution to HQ with the value over 1.0, indicating that Cl was the most hazardous elemental species for children and adults' health. Hence, the emissions of Cl-related industries such as waste incineration should be especially given priority for making appropriate control measures. Similar result was also found by Slezakova et al. (2014) that As and Cl were the first two dominant contributors (~ 90%) to noncarcinogenic risks for children and adults in a Portuguese hospital. It should be noted that in this study, HQs of all elemental species for children were slightly higher than those of adults. This was different from previous works that no difference of HQ between children and adults was found, which was due to that the differences of body weight and inhalation rate were not considered in their calculations of HQ (Hu et al., 2012; Gupta et al., 2020).

Though the HQ values of some heavy metals like As and Mn were below the threshold, their values were over 0.1, which also indicated potential health risk. Compared to Pre-Lock and Post-Lock, the HQ values of some elements such as Cr (VI), Mn, As, Zn, V, and Ni were lower during COVID-Lock, indicating that the lockdown measures were beneficial for

lowering the non-carcinogenic risk to a certain extent. One exception was for Cl that its HQ was the highest during COVID-Lock, which was attributed to the higher Cl ambient concentrations during this period.

Carcinogenic risk assessment from specific elements is shown in **Fig. 5b**. Here, six heavy metals that had carcinogenic effects were assessed and their accumulated risks were also calculated. TR values of all metal species were below the acceptable level (10^{-6}) for children, indicating that the carcinogenic risk posed by those toxic elements to children via inhalation was not serious. However, the cumulative carcinogenic risk of these heavy metals was close to 1, indicating that these heavy metals had collective carcinogenic risk for children.

Different from the carcinogenic risk of heavy metal for children, TR (target carcinogenic risk) values of As and the accumulated risks were higher than the safety level (10^{-6}) for adults during all three periods. During Pre-Lock, TR of the assessed elements followed the order of As > Cr (VI) > Cd > Ni > Co > Pb. It was As > Cr (VI) > Cd > Ni > Co > Pb during the COVID-Lock and As > Cr (VI) > Cd > Ni > Co > Pb during Post-Lock, respectively. Cr and As were the two greatest contributors to TR during Pre-Lock and Post-Lock, indicating that manufacture processing and coal combustion were the predominant sources to carcinogenic risk. While during the COVID-Lock, As was the largest contributor to carcinogenic risk, which was due to the large reduction of industrial activities during the lockdown. This result was similar to one previous work that coal combustion was identified as the most important contributor to the health risk in Beijing because of the higher toxicity elements (As and Cd) emitted (Liu et al., 2018).

As discussed above, the non-carcinogenic risk for children was slightly higher than that for adults. In contrast, the carcinogenic risk for adults was much higher than that for children. This should be due to the individual body differences such as inhalation rate, body weight, and exposure time (Slezakova et al., 2014; Gao et al., 2017). Compared to the higher non-carcinogenic risk during COVID-Lock, carcinogenic risk was the lowest during the same period, owing to reduction of most heavy metals. However, the extent of TR reduction was not significant and the total TR largely exceeded the acceptable risk level. Therefore, a substantial and lasting emission reduction of heavy metals should be enacted to lower the carcinogenic risk.

2.4.2 Source-based health risk assessment

In this section, we further assessed the source-oriented health risk for children and adults based on the PMF modeling results. As shown in **Fig. 6a**, waste incineration had the highest

HQ values among the five identified sources during the three periods and exceeded the threshold of 1.0 for children, indicating the potential non-carcinogenic health effects from this emission sector. Moreover, HQ values from waste incineration during COVID-Lock period were higher than Pre-Lock and Post-Lock, which was ascribed to the dominance of Cl and its higher mass concentrations during the lockdown. Coal combustion ranked the second place, followed by manufacture processing, shipping emission, and fugitive/mineral dust. Since HQ values of these four sources were below the threshold, their impacts on non-carcinogenic risk were considered not strong. For the sake of human health, special attention should be paid to the reduction of Cl-related anthropogenic activities especially from waste incineration.

Fig. 6b shows the source-oriented carcinogenic risk. Different from the non-carcinogenic risk assessment, manufacture processing and coal combustion ranked as the two most important emission sources of carcinogenic risk. As discussed earlier, coal combustion and manufacture processing were rich in As and Cr, respectively, which were the most outstanding toxic metal species contributing to the TR values. The TR values for children from all sources were lower than the acceptable level (10^{-6}) during the whole study period, suggesting almost no potential health risk for children. As for adults, TR from coal combustion was much higher than the acceptable level, implying crucial impact on adults' health. Compared to Pre-Lock and Post-Lock, TR showed significant decline from manufacture processing and was lower than the acceptable level during COVID-Lock, indicating the strict lockdown measures were beneficial for lowering the carcinogenic risk from the industrial sector. As a comparison, this effect was not obvious from the other major emission sectors. Special attention should be paid to shipping emission as its TR was the third highest and close to the acceptable level. Considering that Shanghai is the hub of numerous international shipping lines and the capacity of Shanghai port has been expanding in recent years, it is expected that in the near future, shipping emissions will remain a steady source of the human health risk.

2.5 Emission control priorities from the perspective of pollution sources and health risk assessment

Based on the aforementioned analyses, we proposed pollution reduction strategies based on source apportionment and health risk assessment (**Fig. 7**). From the view of the source contributions to the mass loadings of $PM_{2.5}$-bound elemental species, additional restrictions should be placed on coal combustion. Adjusting the energy structure may be the practical way to reduce coal-fired pollution, such as the change of coal to natural gas. Also, control measures on shipping emission in coastal regions should be carried out, such as lowering the

emission limit of pollutants from offshore ships, improving the quality of oil used by ships, and setting up offshore shipping emission buffer zone.

From the perspective of health risk, the emission control priorities should think highly of source contributions to health risk rather than source contributions to the ambient concentrations of elements only. Although coal combustion dominated the mass concentrations of elemental species in $PM_{2.5}$, its health risk was not the highest. Instead, waste incineration was found contributing the most to non-carcinogenic risk, highlighting the importance of emission control on the waste incineration. For carcinogenic risk, the priority of pollutant emission reduction should focus on manufacturing process and coal combustion. This study also pointed out shipping emissions as a potential source affecting the health risk of residents in coastal regions. Overall, it is proposed that a balanced way should be reached between both lowering the levels of air pollutants and their health risks.

3 Conclusions

During the COVID-19 pandemic, real-time measurements of trace elemental species at a coastal site of Shanghai was conducted. Most trace elemental species in $PM_{2.5}$ showed different extents of reductions during the lockdown. The diel patterns of all the trace elemental species showed obvious diel cycles with higher values in the daytime and lower values at night before the lockdown. However, either flat or irregular diel patterns without showing discernable peaks were observed during the lockdown. Remarkable reductions of anthropogenic emissions from both land and waters during the lockdown were found, e.g. from industrial emissions (Cr, Mn, and Zn as tracers), fugitive/mineral dust (Ca and Fe as tracers), and shipping emissions (V and Ni as tracers). Cl was an exception that had higher concentrations during the lockdown, which may be related to the increase of waste incineration caused by more domestic waste from living at home during quarantine. Most trace elemental species rebounded rapidly after the lockdown, indicating the recovery of anthropogenic emissions. Specifically, the levels of V and Ni even exceeded those before the lockdown.

PMF receptor model was applied to apportion the pollution sources of $PM_{2.5}$-bound elemental species. Five major sources were identified according to the typical tracers. Coal combustion contributed over 70% to the measured elemental species before and during the lockdown. Waste incineration displayed an increased contribution during COVID-Lock. After the lockdown, contributions from shipping emissions, waste incineration, fugitive/mineral dust,

and manufacture processing all rebounded strongly, resulting in a decreased contribution from coal combustion.

The total non-carcinogenic risk (HQ) from the investigated elements exceeded the threshold (1.0) before, during, and after the lockdown for both children and adults, of which Cl was the predominant species contributing to HQ. Whereas, the total target carcinogenic risk (TR) was higher than the acceptable level (10^{-6}) for adults, while the total TR for children was below the safety level. As and Cr (VI) ranked as the two most important elemental species contributing to TR and their carcinogenic risk for adults were higher than for children. From the perspective of source apportionment, waste incineration was the largest contributor to HQ, while manufacture processing and coal combustion were the main contributors to TR for children and adults.

This study provided a multidimensional solution for air pollution control, that is, from the view of the source contributions to the mass loadings of $PM_{2.5}$-bound elemental species, additional restrictions should be placed on coal combustion. While from the perspective of health risk, priority should be given to control the pollution sources related to waste incineration, manufacture processing and coal combustion. Reduction of shipping emission also should be considered in the coastal regions (e.g. Shanghai) in the future works to reduce the health effects of toxic metals, such V and Ni.

Declaration of interests

The authors declare that they have no known competing financial interests or personal relationships that could have appeared to influence the work reported in this paper.

Acknowledgments

This work was financially supported by the National Key R&D Program of China (No. 2018YFC0213105), the National Science Foundation of China (grant no. 91644105), and the Natural Science Foundation of Shanghai (18230722600, 19ZR1421100, 20ZR1422000). Kan Huang also acknowledges Jiangsu Shuangchuang Program through Jiangsu Fuyu Environmental Technology Co., Ltd.

References

Amato, F., Schaap. M., Denier van der Gon, Hugo A.C., Pandolfi, M., Alastuey. A., et al., 2013. Short term variability of mineral dust, metals and carbon emission from road dust resuspension, Atmos. Environ. 74, 134–140.

Bartoňová, L., Raclavská, H., Čech, B., Kucbel, M., 2019. Behavior of Pb during coal combustion: An overview. Sustainability 11, 6061.

Bauwens, M., Compernolle, S., Stavrakou, T., Müller, J.F., van Gent, J., Eskes, H., et al., 2020. Impact of coronavirus outbreak on NO_2 pollution assessed using TROPOMI and OMI observations. Geophys.Res. Lett. 47, e2020GL087978.

Chang, Y.H., Huang, K., Xie, M.J., Deng, C.R., Zou, Z., Liu, S.D., et al., 2018. First long–term and near real-time measurement of trace elements in China's urban atmosphere: temporal variability, source apportionment and precipitation effect. Atmos. Chem. Phys. 18, 11793–11812.

Chen, C.R., Lai, H.C., Liao, M.I., Hsiao, M.C., Ma, H.W., et al., 2021. Health risk assessment of trace elements of ambient $PM_{2.5}$ under monsoon patterns. Chemosphere, 264, 128462.

Cheng, Y., Engling, G., He, K.B., Duan. F.K., Ma, Y.L., Du, Z.Y., et al., 2013. Biomass burning contribution to Beijing aerosol. Atmos. Chem. Phys. 13, 7765–7781.

Cimova, N., Novak, M., Chrastny, V., Curik, J., Veselovsky. F., Blaha, V., et al., 2016. Lead fluxes and 206Pb/207Pb isotope ratios in rime and snow collected at remote mountain–top locations (Czech Republic, Central Europe): patterns and sources. Atmos. Environ. 143, 51–59.

Fu, X., Wang, T., Wang, S.X., Zhang, L., Cai, S.Y., Xing, J., et al., 2018. Anthropogenic Emissions of Hydrogen Chloride and Fine Particulate Chloride in China. Environ. Sci. Technol. 52, 1644–1654.

Gao, J.J., Tian, H.Z., Cheng, K., Lu, L., Wang, Y.X., Wu, Y., et al, 2014. Seasonal and spatial variation of trace elements in multi-size airborne particulate matters of Beijing, China: mass concentration, enrichment characteristics, source apportionment, chemical speciation and bioavailability. Atmos. Environ. 99, 257–265.

Gao, P., Lei, T.T., Jia, L.M., Song, Y., Lin, N., Du, Y.Q., et al., 2017. Exposure and health risk assessment of $PM_{2.5}$-bound trace metals during winter in university campus in Northeast China. Sci. Total Environ. 576, 628–636.

Gelado-Caballero, M.D., López-García, P., Prieto, S., Patey, M.D., Collado, C., Hérnández-Brito. J.J., 2012. Long- term aerosol measurements in Gran Canaria, Canary Islands: Particle concentration, sources and elemental composition, J. Geophys. Res. 117, D03304.

Gupta. P., Satsangi, M., Satsangi, G.P., Jangid, A., Liu, Y., Pani, S.K., et al., 2020. Exposure to respirable and fine dust particle over North-Central India: chemical characterization, source interpretation, and health risk analysis. Environ Geochem Health. 42, 2081–2099.

Health Effects Institute, 2020. State of Global Air 2020. Special Report. Boston, MA: Health Effects Institute. Available: https://www.healtheffects.org/annual-report-2020

Hu, X., Zhang, Y., Ding, Z.H., Wang, T.J., Lian, H.Z., Sun, Y.Y., et al., 2012. Bioaccessibility and health risk of arsenic and heavy metals (Cd, Co, Cr, Cu, Ni, Pb, Zn and Mn) in TSP and $PM_{2.5}$ in Nanjing, China. Atmos. Environ. 57, 146–152.

Hsu, C.Y., Chiang, H.C., Lin, S.L., Chen, M.J., Lin, T.Y., Chen, Y.C., et al., 2016. Elemental characterization and source apportionment of PM_{10} and $PM_{2.5}$ in the western coastal area of central Taiwan. Sci. Total Environ. 541, 1139–1150.

Huang, X., Ding, A.J., Gao, J., Zheng, B., Zhou, D.R., Qi, X.M., et al., 2020. Enhanced secondary pollution offset reduction of primary emissions during COVID–19 lockdown in China, Natl. Sci. Rev. 0, 1–9.

IARC Working Group on the Evaluation of Carcinogenic Risks to Humans, 2006. Inorganic and organic lead compounds. IARC Monogr Eval Carcinog Risks Hum. 87, 1–471

IARC Working Group on the Evaluation of Carcinogenic Risks to Humans, 2012. Arsenic, metals, fibres, and dusts. IARC Monogr Eval Carcinog Risks Hum. 100 (Pt C), 11–465.

Li, L., Li, Q., Huang, L., Wang, Q., Zhu, A.S., Xu, J., et al., 2020. Air quality changes during the COVID-19 lockdown over the Yangtze River Delta Region: An insight into the impact of human activity pattern changes on air pollution variation. Sci. Total Environ. 732, 139282.

Liu, J.W., Chen, Y.J., Chao, S.H., Cao, H.B., Zhang, A.C., Yang. Y., 2018. Emission control priority of $PM_{2.5}$-bound heavy metals in different seasons: a comprehensive analysis from health risk perspective. Sci. Total Environ. 644, 20–30.

Liu, Y.M., Fan, Q., Chen, X.Y., Zhao, J., Ling, Z.H., Hong, Y.Y., et al., 2018. Modeling the impact of chlorine emissions from coal combustion and prescribed waste incineration on tropospheric ozone formation in China. Atmos. Chem. Phys. 18, 2709–2724.

McCulloch, A., Aucott, M.L., Benkovitz, C.M., Graedel, T.E., Kleiman, G., Midgley, P.M., et al., 1999. Global emissions of hydrogen chloride and chloromethane from coal combustion, incineration and industrial activities: Reactive Chlorine Emissions Inventory. J. Geophys. Res. 104 (D7), 8391–8403.

Nriagu, J.O., 1989. A global assessment of natural sources of atmospheric trace metals. Nature. 338, 47–49.

Okuda, T., Katsuno, M., Naoi, D., Nakao, S., Tanaka, S., He, K.B., et al., 2008. Trends in hazardous trace metal concentrations in aerosols collected in Beijing, China from 2001 to 2006. Chemosphere 72, 917–924.

Paatero, P., Tapper, U., 1994. Positive matrix factorization: A non-negative factor model with optimal utilization of error estimates of data values. Environmetrics 5, 111–126.

Paatero, P., Eberly, S., Brown, S.G., Norris, G.A., 2014. Methods for estimating uncertainty in factor analytic solutions. Atmos. Meas. Tech. 7, 781–797.

Pachon, J.E., Weber, R.J., Zhang, X.L., Mulholland, J.A., Russell, A.G., 2013. Revising the use of potassium (K) in the source apportionment of $PM_{2.5}$. Atmospheric Pollut. Res. 4(1), 14–21.

Pandolfi, M., Gonzalez–Castanedo, Y., Andrés, A., de la Rosa, J.D., Mantilla, E., Sanchez de la Campa, A., et al., Moreno, T., 2011. Source apportionment of PM_{10} and $PM_{2.5}$ at multiple sites in the strait of Gibraltar by PMF: Impact of shipping emissions. Environ Sci Pollut Res. 18(2), 260–269.

Park, S.S., Cho, S.Y., Jo, M.R., Gong, B.J., Park J.S., Lee, S.J., 2014. Field evaluation of a near-real time elemental monitor and identification of element sources observed at an air monitoring supersite in Korea. Atmospheric Pollut. Res. 5, 119–128.

Pérez, N., Pey, J., Reche, C., Cortés, J., Alastuey, A., Querol X., 2016. Impact of harbour emissions on ambient PM_{10} and $PM_{2.5}$ in Barcelona (Spain): Evidences of secondary aerosol formation within the urban area. Sci. Total Environ. 571, 237–250.

Shelley, R.U., Morton, P.L., Landing, W.M., 2015. Elemental ratios and enrichment factors in aerosols from the US–GEOTRACES North Atlantic transects. Deep Sea Res. Part II. 116, 262–272.

Shi, X.Q., Brasseur, G.P., 2020. The response in air quality to the reduction of Chinese economic activities during the COVID-19 outbreak. Geophys.Res. Lett. 47, e2020GL088070.

Slezakova, K., Morais, S., Pereira, M., 2014. Trace metals in size-fractionated particulate matter in a Portuguese hospital: exposure risks assessment and comparisons with other countries. Environ Sci Pollut Res. 21, 3604–3620.

Tian, H.Z., Zhu, C.Y., Gao, J.J., Cheng, K., Hao, J.M., Wang, K., et al., 2015. Quantitative assessment of atmospheric emissions of toxic heavy metals from anthropogenic sources in China: Historical trend, spatial distribution, uncertainties, and control policies, Atmos. Chem. Phys. 15, 10127–10147.

USEPA, 1989. Assessment Guidance for Superfund, Volume 1-Human Health Evaluation Manual (Part A); Interim Final, EPA/540/1-89/002. Office of Emergency and Remedial Response, Washington, DC. https://semspub.epa.gov/work/HQ/191.pdf.

USEPA, 2009. Risk Assessment Guidance for Superfund, Volume I: Human Health Evaluation Manual (Part F, Supplemental Guidance for Inhalation Risk Assessment). https://www.epa.gov/risk/risk-assessment-guidance-superfund-rags-part-f.

USEPA, 2014. EPA Positive Matrix Factorization (PMF) 5.0 Fundamentals and User Guide.

USEPA, 2018. Regional Screening levels (RSLs)-user's guide. Retrieved from https://www.epa.gov/risk/regional-screening-levels-rsls-users-guide. Lasted accessed on 13, September 2021.

Visser, S., Slowik, J.G., Furger, M., Zotter, P., Bukowiecki, N., Dressler, R., et al., 2015. Kerb and urban increment of highly time-resolved trace elements in PM_{10}, $PM_{2.5}$ and $PM_{1.0}$ winter aerosol in London during ClearfLo 2012. Atmos. Chem. Phys. 15, 2367–2386.

Wang, P.F., Chen, K.Y., Zhu, S.Q., Wang, P., Zhang, H.L., 2020. Severe air pollution events not avoided by reduced anthropogenic activities during COVID-19 outbreak. Resour Conserv Recycl. 158, 104814.

Wedepohl, K.H., 1995. The composition of the continental crust. Geochimica et Cosmochimica Acta. 59 (7), 1217–1232.

Wei, Y., Liu, G.J., Fu, B., Wang, R.W., Liu, Y., Xue, X., et al., 2021. Partitioning behavior of Pb in particulate matter emitted from circulating fluidized bed coal-fired power plant. J. Clean. Prod. 292, 125997.

WHO, 2020. Novel Coronavirus (2019-nCoV) Situation Report-22, World Health Organization, https://www.who.int/docs/default-source/coronaviruse/situation-reports/20200211-sitrep-22-ncov.pdf.

Wu, F., Zhao, S., Yu, B., Chen, Y.M., Wang, W., Song, Z.G., et al., 2020. A new coronavirus associated with human respiratory disease in China. Nature. 579, 265–269.

Yang, H.N., Chen, J., Wen, J.J., Tian, H.Z., Liu, X.G., 2016. Composition and sources of $PM_{2.5}$ around the heating periods of 2013 and 2014 in Beijing: implications for efficient mitigation measures. Atmos. Environ. 124, 378–386.

Yu, J.J, Yan, C.Q, Liu, Y., Li, X.Y., Zhou, T., Zheng, M., 2018. Potassium: A Tracer for Biomass Burning in Beijing? Aerosol Air Qual. Res. 18, 2447–2459.

Zhang, R., Jing, J., Tao, J., Hsu, S.C., Wang, G, Cao, J., et al., 2013. Chemical characterization and source apportionment of $PM_{2.5}$ in Beijing: seasonal perspective. Atmos. Chem. Phys. 13, 7053–7074.

Zhao, M.J., Zhang, Y., Ma, W.C., Fu, Q.Y., Yang, X., Li, C.L., et al., 2013. Characteristics and ship traffic source identification of air pollutants in China's largest port. Atmos. Environ. 64, 277–286.

Zhou, P., Yang, X.L., Wang, X.G., Hu, B., Zhang, L., Zhang, W., et al., 2020. A pneumonia outbreak associated with a new coronavirus of probable bat origin. Nature. 579, 270–273.

Zhu, N., Zhang, D.Y., Wang, W.L, Li, X.W., Yang, B., Song, J.D., et al., 2020. A novel coronavirus from patients with pneumonia in China, 2019. N. Engl. J. Med. 382, 727–733.

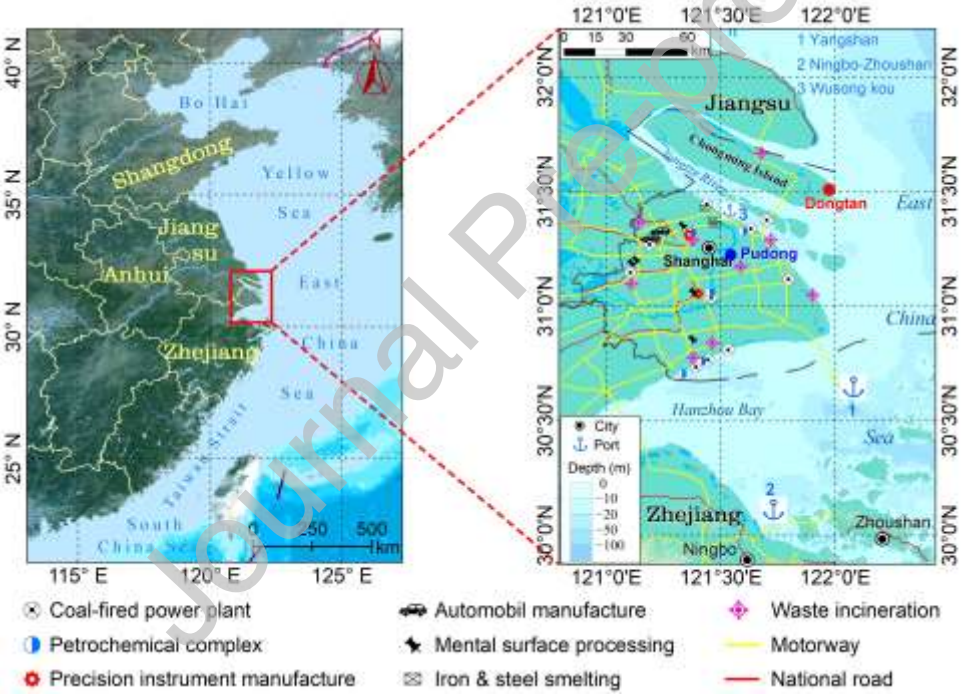

Fig. 1 The observational sites in this study. The red and blue filled circles represent the coastal site (Dongtan) and the urban site (Pudong) in Shanghai, respectively. And the major point pollution sources except waste incineration were modified from Chang et al., (2018) and vectored by ArcGIS 10.3 (Esri, USA).

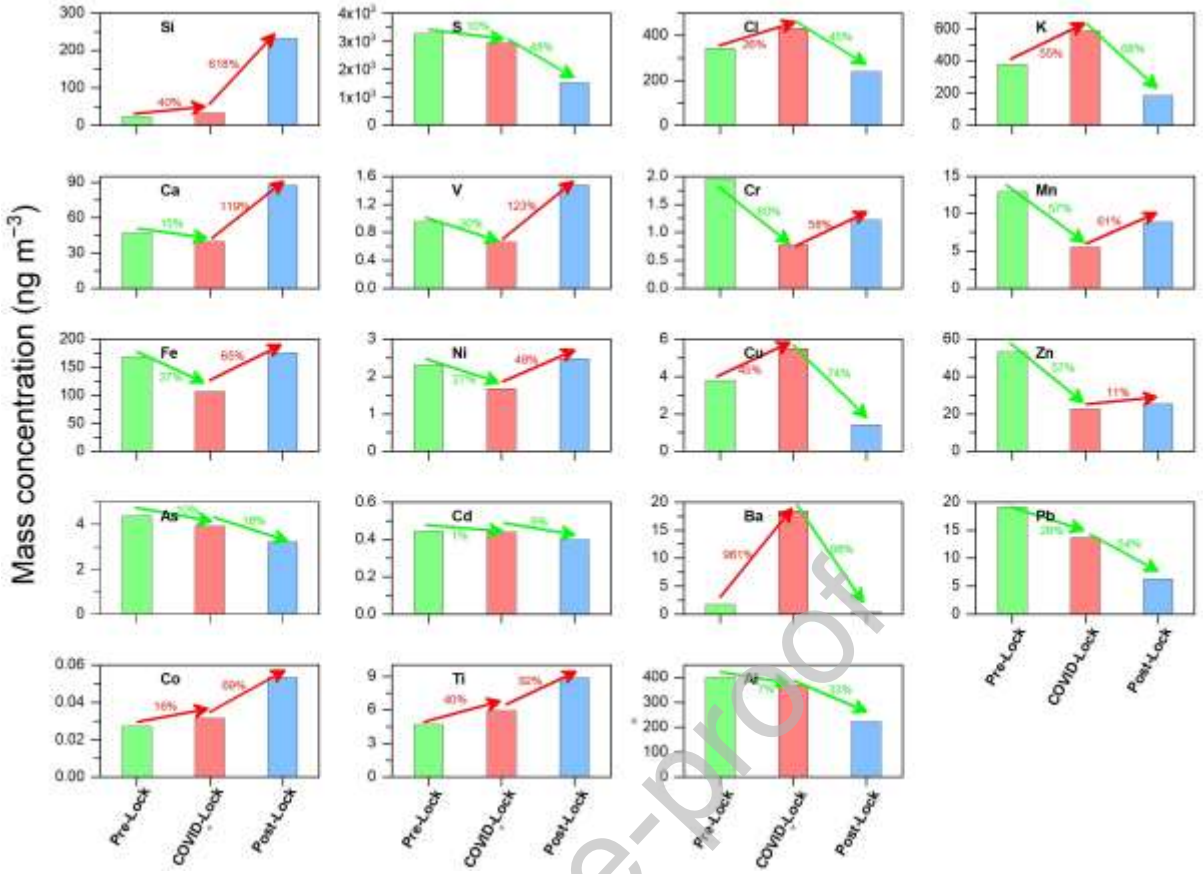

Fig. 2 Variation of the mass concentrations of 19 elemental species in $PM_{2.5}$ at Dongtan before, during, and after the COVID-19 lockdowns. The green arrows and numbers represent the reduction percentages while the red arrows and numbers represent the increase percentages.

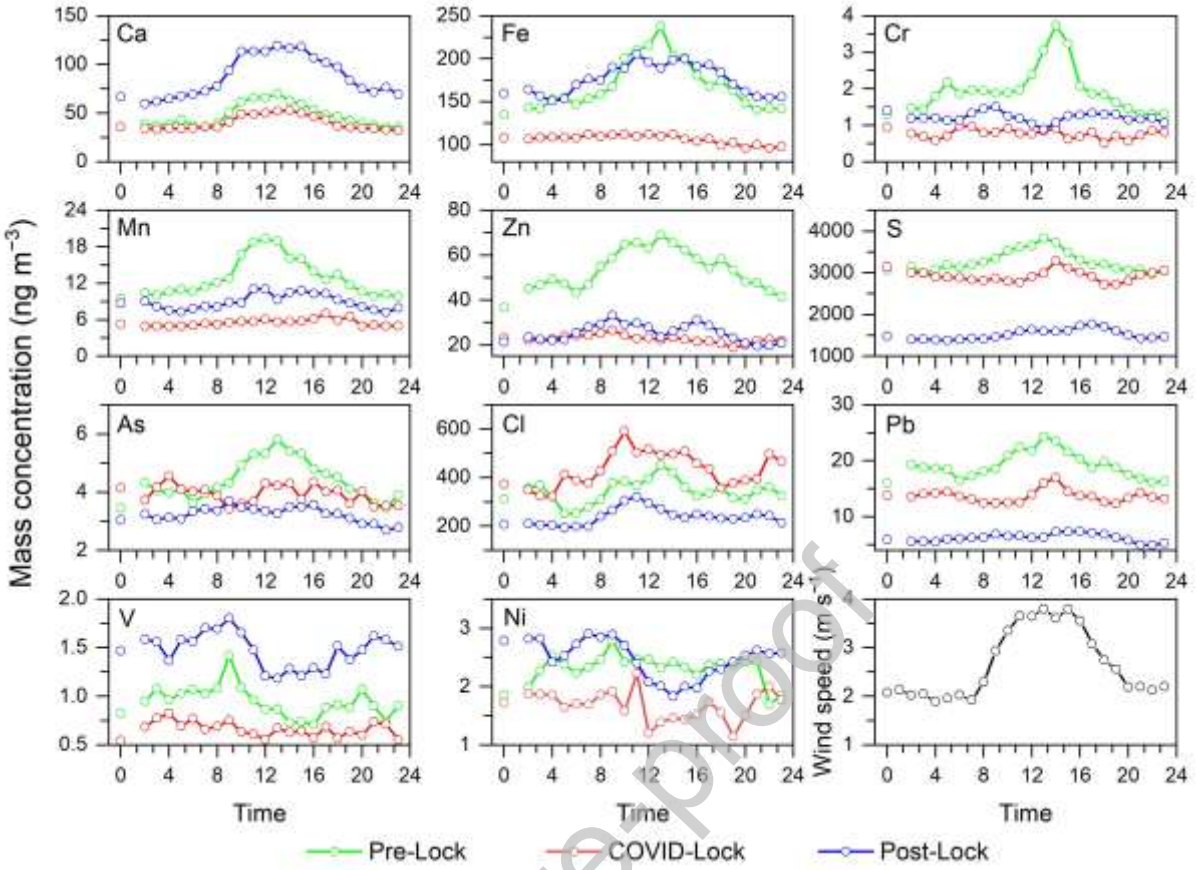

Fig. 3 Diel patterns of major trace elemental species before, during, and after the COVID-19 lockdowns and wind speed in the whole study period at Dongtan (the missing data at 1:00 was due to the maintenance of instrument).

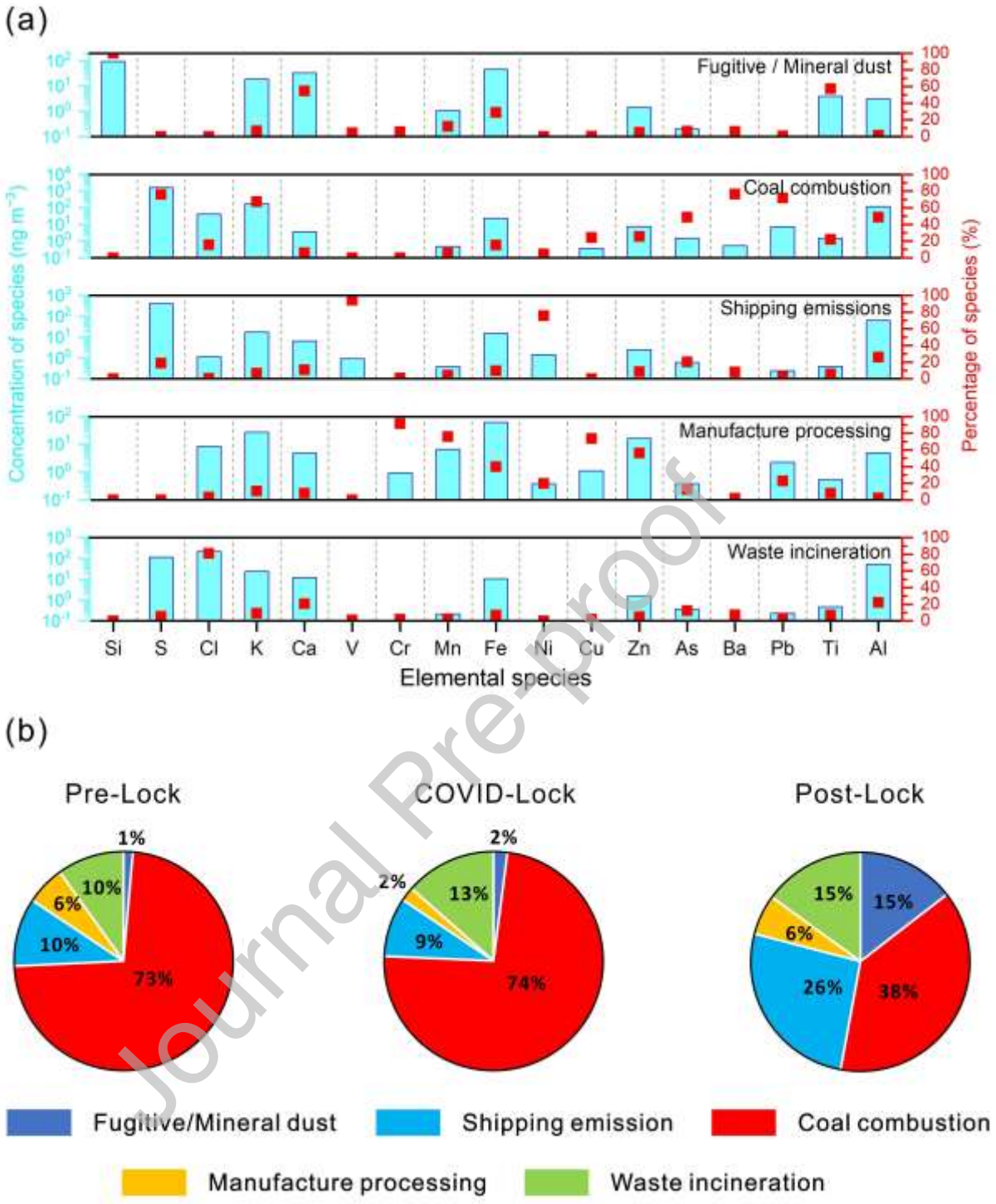

Fig. 4 Source contribution results identified by PMF receptor model. (a) source profiles (concentration and percentage of species) of $PM_{2.5}$-bound elemental species; (b) source contributions to $PM_{2.5}$-bound elemental species.

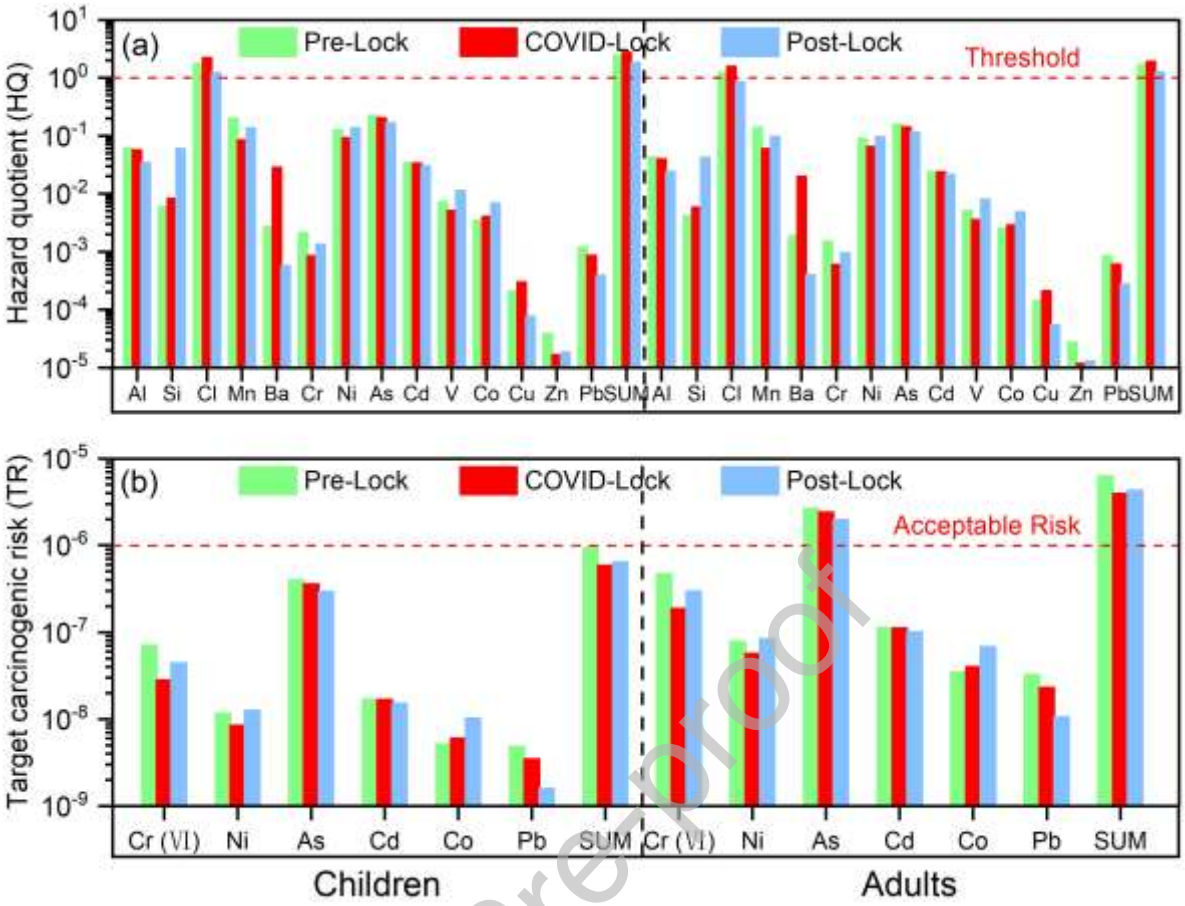

Fig. 5 Health risks assessment from specific elements. (a) non-carcinogenic risk and (b) target carcinogenic risk. Cr in (a) was calculated by using Cr (VI).

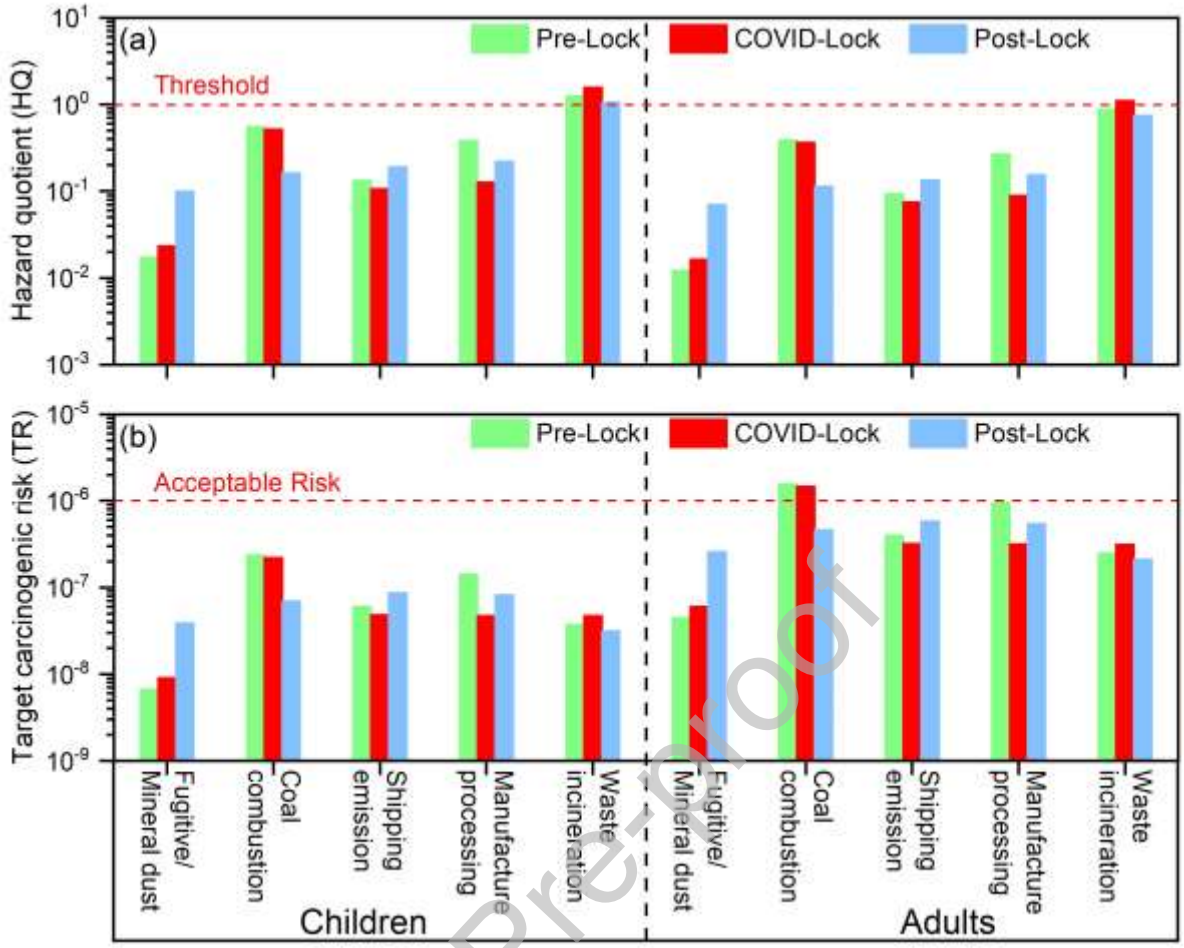

Fig. 6 Estimated health risks risk from different sources identified by PMF model. (a) non-carcinogenic risk and (b) carcinogenic risk.

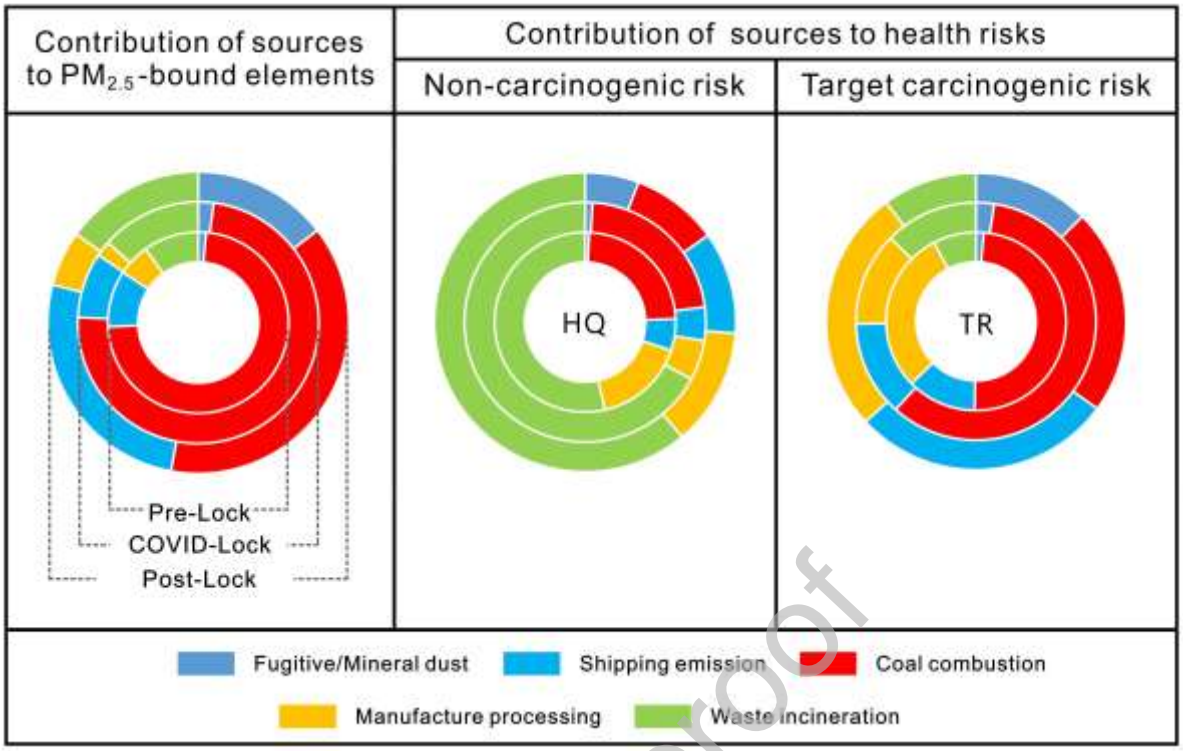

Fig. 7 A summary of contributions of emission sources to $PM_{2.5}$-bound trace elements and associated health risks